Journal of Alloys and Compounds 484 (2009) 59–68

Contents lists available at ScienceDirect

Journal of Alloys and Compounds

journal homepage: www.elsevier.com/locate/jallcom

Hexagonal $LMn_6Sn_4Ge_2$ investigated by neutron diffraction and ^{119}Sn Mössbauer spectroscopy (L = Tb, Ho, Lu)

G. Venturini [a,*], B. Malaman [a], Laura K. Perry [b], D.H. Ryan [b]

[a] Laboratoire de Chimie du Solide Minéral, Institut Jean Lamour (UMR 7198) Faculté des Sciences et Techniques, B.P. 239, 54506 Vandoeuvre les Nancy Cedex, France
[b] Centre for the Physics of Materials and Physics Department, McGill University, 3600 University Street, Montréal, Quebec H3A 2T8, Canada

ARTICLE INFO

Article history:
Received 29 April 2009
Received in revised form 12 May 2009
Accepted 16 May 2009
Available online 23 May 2009

Keywords:
Lanthanoid alloys and compounds
Transition metal alloys and compounds
Mössbauer spectroscopy
Neutron diffraction

ABSTRACT

The hexagonal compounds $LMn_6Sn_4Ge_2$ (L = Tb, Ho, Lu) have been investigated by neutron diffraction and ^{119}Sn Mössbauer spectroscopy. The location of Ge atoms on the 2c site has been confirmed. The $TbMn_6Sn_4Ge_2$ compound is ferrimagnetic and characterized by an easy-plane magnetisation in the whole 2–300 K temperature range. The magnetic moments at 2 K are $\mu_{Tb} = 8.65\mu_B$ and $\mu_{Mn} = 2.36\mu_B$. The $HoMn_6Sn_4Ge_2$ compound is ferrimagnetic and characterized by an easy-plane magnetisation above 130 K and by an easy cone anisotropy below this temperature. The magnetic moments at 2 K are $\mu_{Tb} = 9.26\mu_B$ and $\mu_{Mn} = 2.28\mu_B$ and the angle with respect to the *c* axis is $\theta_c = 51^\circ$. The $LuMn_6Sn_4Ge_2$ compound is helimagnetic in the 2–300 K temperature range with the Mn moment lying in the (0 0 1) plane but around room temperature, it shows some weak lines associated with an antiferromagnetic structure characterized by a doubling of the *c* axis. The magnetic moment at 2 K is $\mu_{Mn} = 2.27\mu_B$. Mössbauer spectroscopy indicates that the Mn slab around the 2(d) Sn site is ferromagnetic. Analysis of the results indicates that replacement of Ge for tin changes the anisotropy direction of the L element probably as a result of a change of the sign of the second order CEF parameter. However, the observation of conical anisotropy of Ho also indicates that the fourth order parameter plays a role.

1. Introduction

Recent studies of hexagonal $HfFe_6Ge_6$-type $LMn_6Sn_4Ge_2$ (L = Sc, Y, Nd–Sm, Gd–Tm, Lu) have revealed interesting features [1]. In the case of the $TmMn_6Sn_4Ge_2$ compound, magnetisation measurements revealed a hard magnetic behaviour suggesting an easy axis anisotropy which has been confirmed more recently using neutron diffraction [2]. On the contrary, the $TbMn_6Sn_4Ge_2$ compound was characterized by a soft magnetic behaviour although the parent compound $TbMn_6Sn_6$ displayed a large coercive field [3]. In order to investigate the relations between the easy magnetisation anisotropy and the sign of the Steven's coefficients we decided to study two other ferrimagnetic compounds, namely $TbMn_6Sn_4Ge_2$ ($T_c = 428$ K) and $HoMn_6Sn_4Ge_2$ ($T_c = 391$ K) using neutron diffraction. Another interesting behaviour of the $TmMn_6Sn_4Ge_2$ compound is the stabilisation of a ferrimagnetic state at low temperature although the parent compounds $TmMn_6Sn_6$ and $TmMn_6Ge_6$ remain helimagnetic down to 2 K [4,5]. This behaviour arises either from a modification of the strength of the antiferromagnetic Mn–Mn interactions in the substituted stannides or from increasing Tm–Mn interactions due to the shorter Tm–Mn distances. For this reason, it was also interesting to check the behaviour of the Mn sublattice alone in a compound involving a non magnetic L element and it has been decided to undertake a neutron diffraction study of the antiferromagnetic $LuMn_6Sn_4Ge_2$ compound ($T_N = 366$ K). Previous studies have shown that the hyperfine parameters derived from ^{119}Sn Mössbauer spectroscopy were very sensitive to the magnetic phenomena occurring in this family of compounds. Therefore, the present compounds have been also characterized by ^{119}Sn Mössbauer spectroscopy.

2. Experimental methods

The compounds were prepared starting from the stoichiometric amounts of lanthanoid, manganese, tin and germanium pieces melted in an induction furnace. The resulting ingot was then annealed for two weeks at 1123 K. The quality of the sample was checked by powder X-ray diffraction analysis using an Phillips XPert Pro diffractometer (Cu Kα). The neutron diffraction patterns were recorded on the D1b spectrometer (λ = 2.52 Å) at the Institut Laue-Langevin (ILL Grenoble) and the magnetic structures were refined with the FULLPROF software [6].

^{119}Sn Mössbauer spectra were collected in transmission mode on a constant acceleration spectrometer using a 0.4 GBq ^{119m}Sn $CaSnO_3$ source with the powdered samples mounted in a vibration-isolated closed-cycle refrigerator. A 25 μm Pd filter was used to absorb the Sn Kα X-rays also emitted by the source. The spectrometer was calibrated using a ^{57}Co Rh source and an αFe foil. A $CaSnO_3$ standard gave a spectrometer linewidth of 0.6 mm/s full width at half maximum (FWHM). Isomer shifts were measured relative $CaSnO_3$. The $LMn_6Sn_4Ge_2$ compounds all gave slightly

* Corresponding author. Tel.: +33 3 83 68 46 73; fax: +33 3 83 68 46 11.
E-mail address: Gerard.Venturini@lcsm.uhp-nancy.fr (G. Venturini).

0925-8388/$ – see front matter © 2009 Elsevier B.V. All rights reserved.
doi:10.1016/j.jallcom.2009.05.068

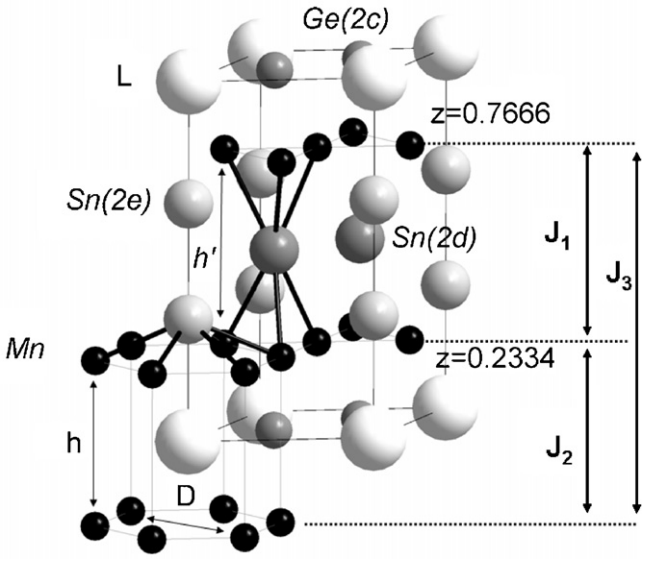

Fig. 1. Representation of the crystal structure of $LMn_6Sn_4Ge_2$. The geometric features of the Mn_{12} hexagonal prism around the L atom are outlined and the description of the interlayer interactions J_i is displayed.

broadened lines (≈0.8 mm/s), although the metallic tin impurity that was present in all three compounds was sharper.

The spectra were fitted using a conventional non-linear least-squares minimisation routine to a sum of Lorentzian lineshapes. The high point symmetries of the three Sn sites in the $HfFe_6Ge_6$-type structure (6*mm* for Sn-2e and $\bar{6}m2$ for Sn-2c and Sn-2d) mean that in all three cases the electric field gradient (*efg*) is axially symmetric ($\eta = 0$) and the principal (z) axis of the *efg* is parallel to the crystallographic *c* axis at each site [7–9]. The resulting quadrupole shift (Δ) in a magnetically split spectrum is given by:

$$\Delta = \frac{eQV_{zz}}{4}(3\cos^2\theta - 1)$$

where θ is the angle between the z-axis of the *efg* and the hyperfine field (B_{hf}) at the Sn site due to the surrounding magnetic moments. For two of the compounds studied here ($TbMn_6Sn_4Ge_2$ and $LuMn_6Sn_4Ge_2$) a first-order perturbation analysis was used to fit the ^{119}Sn Mössbauer spectra and no direct information on θ was obtained. In this case the observed quadrupole shift is more properly denoted by the symbol ε.

However, in order to follow the evolution of the transferred hyperfine fields in $HoMn_6Sn_4Ge_2$ as it changed from easy plane to easy cone on cooling through 130 K, we fitted the line positions and intensities to a full solution to the nuclear Hamiltonian [7]. This approach yielded the angle between the hyperfine magnetic field (B_{hf}) and the principal component of the electric field gradient tensor (V_{zz}) as a direct fitted parameter.

Each spectrum was fitted with five components: Two approximately equal area magnetic sextets with $B_{hf} \approx 28$ T and ≈15 T (at 12 K) corresponding to Sn atoms in the Sn(2d) and Sn(2e) sites respectively. A much weaker sextet (<5% of the total area) with $B_{hf} \approx 30$ T in the three compounds is attributed to a magnetic impurity. A similar area, larger field component ($B_{hf} \approx 33$ T at 12 K) was also found to be present in the $TbMn_6Sn_4Ge_2$ and $HoMn_6Sn_4Ge_2$ spectra. The hyperfine field for this final magnetic component tracked the temperature dependence of the two other Sn(2d) and Sn(2e) subspectra and therefore this subspectrum has been attributed to residual Sn atoms in the Sn(2c) site that is primarily filled by Ge atoms. A careful analysis of the $LuMn_6Sn_4Ge_2$ spectra has suggested that the site of residual Sn atoms in the Sn(2c) was also present in the low temperature experiments but with a much lower hyperfine field ($B_{hf} \approx 24$ T). The fifth component present in the spectra was a singlet with an isomer shift of ≈2.6 mm/s which exhibited a strongly temperature dependent area (it can be seen in Figs. 1a, 2a and 3a as the central line that grows in strength on cooling). This component is attributed to a metallic tin impurity.

3. Results

3.1. Neutron diffraction study

3.1.1. Crystal structure

The neutron diffraction patterns of the $LMn_6Sn_4Ge_2$ compounds studied here are fully consistent with the $HfFe_6Ge_6$-type structure [*P*6/*mmm*; Hf in 1(a) (0,0,0); Fe in 6(i) (1/2,0,*z*); Ge in 2(c) (1/3,2/3,0), 2(d) (1/3,2/3,1/2) and 2(e) (0,0,*z*)]. The results of the room temperature refinements of the atomic coordinates and site occupation are given in Table 1 together with the atomic coordinates for $TbMn_6Sn_6$ [10]. As previously observed, the Ge atoms are localized in the 2(c) site and the Sn atoms in the 2(d) and 2(e) sites (Fig. 1). This occupation leads to a considerable change of the z_{Mn} coordinate with respect to that measured in the ternary stannides and, in turn, sig-

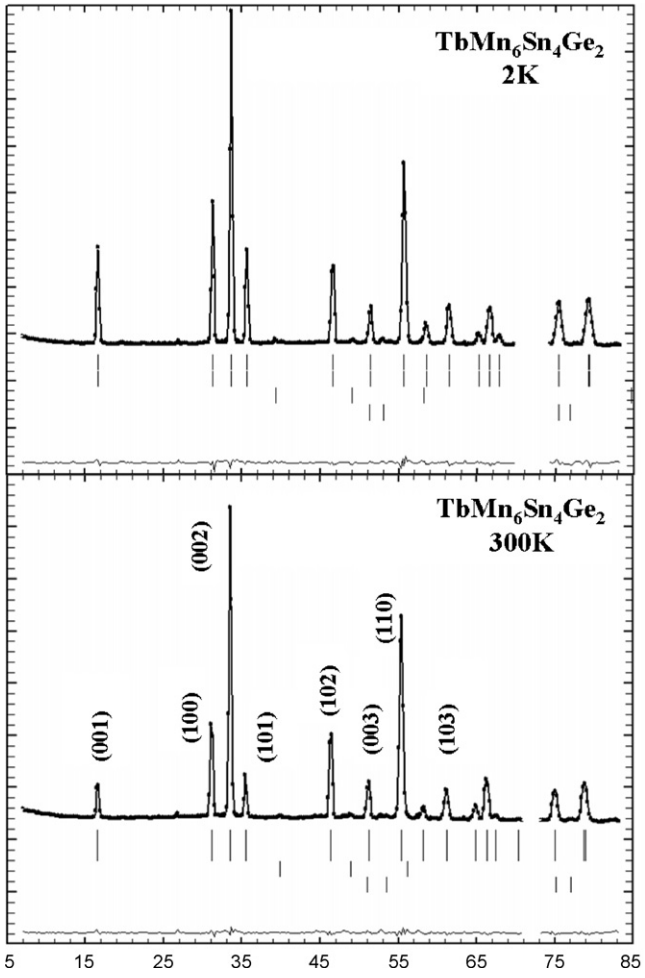

Fig. 2. Observed and calculated neutron diffraction spectra of $TbMn_6Sn_4Ge_2$ at 2 and 300 K. The two lower lines of ticks correspond to the impurities: (from bottom to top) Sn, Mn_2Sn.

Table 1
Neutron data of $LMn_6Sn_4Ge_2$ compounds at room temperature (L = Tb, Ho, Lu) and comparison with the ternary compound $TbMn_6Sn_6$ [10] (see Fig. 1[a]).

	$TbMn_6Sn_4Ge_2$	$HoMn_6Sn_4Ge_2$	$LuMn_6Sn_4Ge_2$	$TbMn_6Sn_6$
a (Å)	5.410(1)	5.400(1)	5.384(1)	5.53
c (Å)	8.725(1)	8.706(1)	8.676(1)	9.023
c/a	1.6127	1.6122	1.6114	1.6316
z_{Mn}	0.2352(6)	0.2334(7)	0.2319(7)	0.2475
z_{Sn2e}	0.3324(9)	0.3337(8)	0.3287(8)	0.3376
Occ (Sn_{2d})	1.0	1.0	1.0	1
Occ (Ge_{2c})	0.99(1)	0.99(1)	0.98(1)	0
Occ (Sn_{2e})	1.0	1.0	1.0	1
$d_{Mn\text{-}2c}$ (Å)	2.579	2.561	2.542	2.745
$d_{Mn\text{-}2d}$ (Å)	2.789	2.796	2.797	2.782
$d_{Mn\text{-}2e}$ (Å)	2.835	2.838	2.820	2.882
$d_{L\text{-}Mn}$ (Å)	3.395	3.379	3.361	3.554
D (Å)[a]	5.410	5.400	5.384	5.53
h (Å)[a]	4.104	4.064	4.024	4.466
h' (Å)[a]	4.621	4.642	4.652	4.557
h/D	0.759	0.753	0.747	0.808

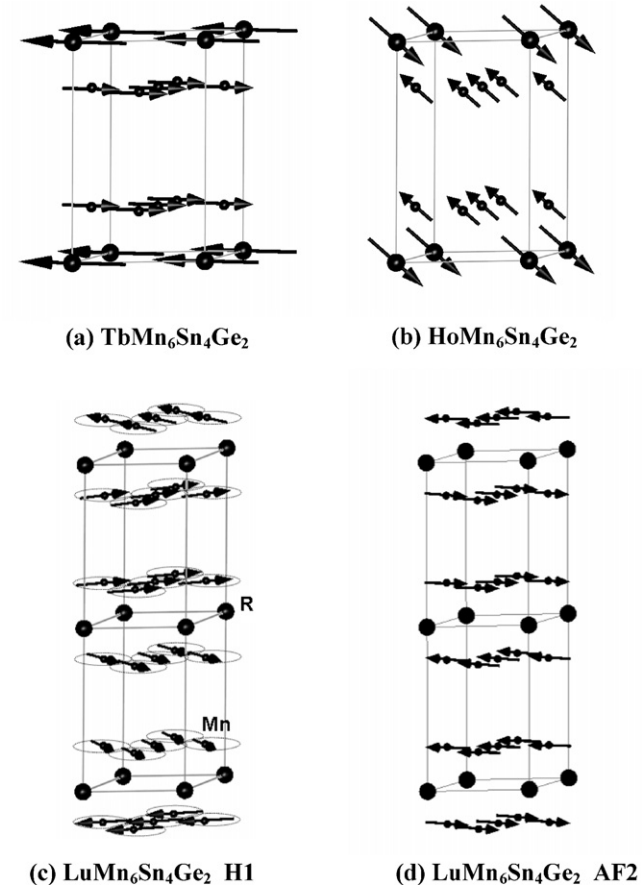

Fig. 3. Representation of the magnetic structures of: (a) in-plane ferrimagnetic for $TbMn_6Sn_4Ge_2$; (b) cone ferrimagnetic for $HoMn_6Sn_4Ge_2$; (c) in-plane helimagnetic for $LuMn_6Sn_4Ge_2$; (d) in-plane antiferromagnetic for $LuMn_6Sn_4Ge_2$.

nificantly modifies some interatomic distances and coordination shells (Table 1). Firstly, we observed that the distances between the Mn atom and the atoms located in 2(c) and 2(d) sites are considerably disproportioned with respect to those observed in ternary $TbMn_6Sn_6$. This is related to the displacement of the Mn atoms and, of course, is consistent with the smaller atomic size of the germanium atom. Secondly, as a consequence of the displacement of the Mn atoms, we also observed a considerable decrease of the L-Mn distance that lead to a significant change in the shape of the hexagonal Mn_{12} prism surrounding the lanthanoid atom. From a magnetic point of view, the $LMn_6Sn_4Ge_2$ structures are characterized by a stacking along *c* of Kagomé planes of manganese building two kinds of slabs: the so-called Mn–Sn–Sn–Sn–Mn slab around the Sn 2(d) site and Mn–(Ge,L)–Mn slab around the Ge 2(c) site.

3.1.2. Magnetic structures of $TbMn_6Sn_4Ge_2$

Two long duration diffraction patterns have been recorded at 300 and 2 K and short duration patterns have been recorded over the whole 2–300 K temperature range. They only display the characteristic nuclear lines of the $HfFe_6Ge_6$ structure (Fig. 2). However, the intensity of the (0 0 1) line is always significantly larger than the intensity expected from the nuclear contribution alone thus indicating that the moments are not aligned along the *c* axis at any temperature, contrary to that observed earlier in the parent compound $TbMn_6Sn_6$ [11]. Refinements assuming a ferrimagnetic structure resulting from a collinear ferromagnetic manganese sublattice and an antiparallel arrangement of the terbium moments yield low residual factors. Attempts to tilt the moments out of the (0 0 1) plane did not improve the reliability factors. The magnetic

Table 2
Structural and magnetic parameters of $TbMn_6Sn_4Ge_2$ at 300 and 2 K.

	300 K	2 K
a (Å)	5.410(1)	5.386(1)
c (Å)	8.725(1)	8.693(1)
z_{Mn}	0.2352(6)	0.2368(7)
z_{Sn2e}	0.3324(9)	0.3347(14)
Occ_{Sn2d}	1	1
Occ_{Ge2c}	0.99(1)	0.99
Occ_{Sn2e}	1	1
μ_{Mn} (μ_B)	2.05(3)	2.36(4)
μ_{Tb} (μ_B)	5.10(5)	8.65(8)
θ(°)	90	90
R_{Bragg}; R_f	1.91; 2.63	1.91; 1.01
R_{magn}; χ^2	2.92; 18.4	1.88; 46.1

structure therefore consists of a ferrimagnetic arrangement of Mn and Tb moments aligned perpendicular to the *c* axis (Fig. 3). The observed and calculated patterns are displayed in Fig. 2 and the refined parameters are summarized in Table 2. The short duration patterns confirm that the moments do not leave the (0 0 1) plane in the whole 2–300 K range and enable us to draw the thermal variation of the magnetic moments (Fig. 4). We will see in Section 3.2 that Mössbauer spectroscopy confirms these conclusions.

3.1.3. Magnetic structures of $HoMn_6Sn_4Ge_2$

The diffraction patterns recorded at 300, 200 and 2 K only display the characteristic nuclear lines of the $HfFe_6Ge_6$ structure (Fig. 5). The intensity of the (0 0 1) line is significantly larger than the intensity of the nuclear contribution alone thus indicating that the moments are not aligned along the *c* axis at any temperature. However, according to previous magnetisation measurements, the thermomagnetic curve of $HoMn_6Sn_4Ge_2$ displays an anomaly around 125 K which might be attributed to a moment reorientation process as observed in the parent compound $HoMn_6Sn_6$ [11]. Fig. 6 displays the thermal variation of some characteristic lines indicating a change below 130 K. Refinements assuming a ferrimagnetic structure resulting from a collinear ferromagnetic manganese sublattice and an antiparallel arrangement of the holmium moment lead to low residual factors. Attempts to tilt the moments out of the (0 0 1) plane do not improve the reliability factor at 300 K and 200 K but significantly reduce it at 2 K and show that the moments make an angle $\theta_c = 51(1)^\circ$ with the [0 0 1] direction at 2 K (Fig. 3).

The thermal variation of the angle θ_c has been checked together with the variation of the magnetic moments. We observed that θ_c

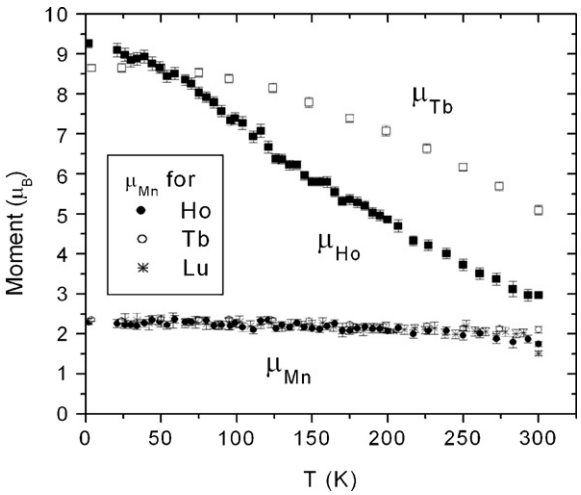

Fig. 4. Thermal variation of the magnetic moments in $LMn_6Sn_4Ge_2$ compounds (L = Tb, Ho, Lu).

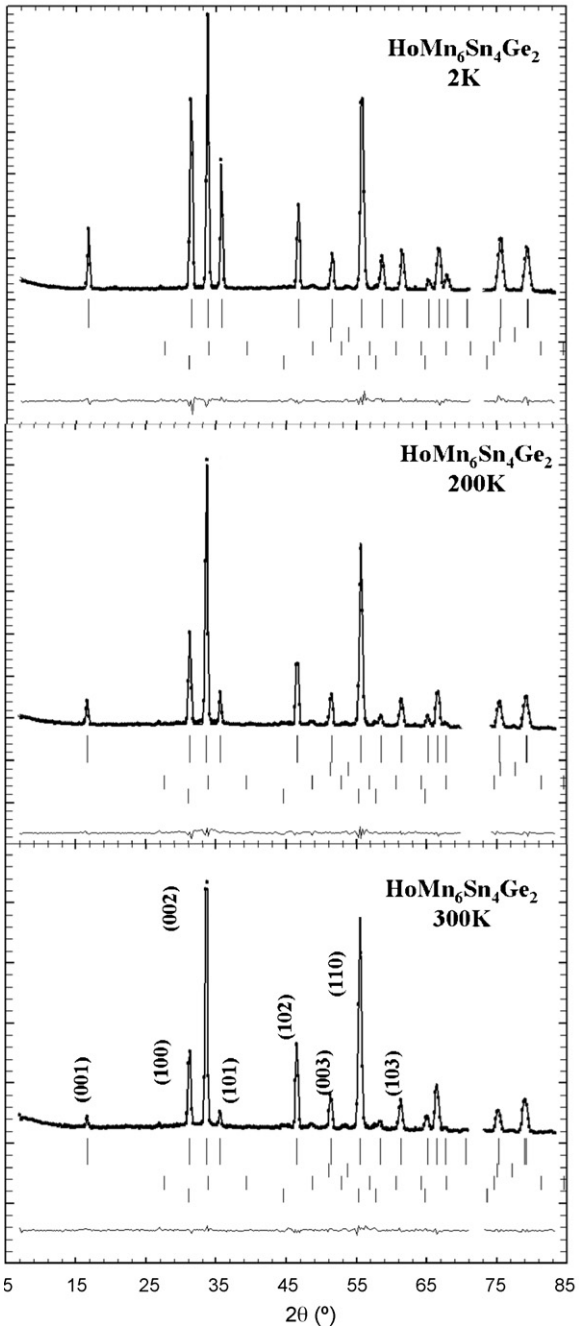

Fig. 5. Observed and calculated neutron diffraction spectra of $HoMn_6Sn_4Ge_2$ at 2 and 300 K. The three lower lines of ticks correspond to the impurities: (from bottom to top) $MnSn_2$, Ho_2O_3, Sn.

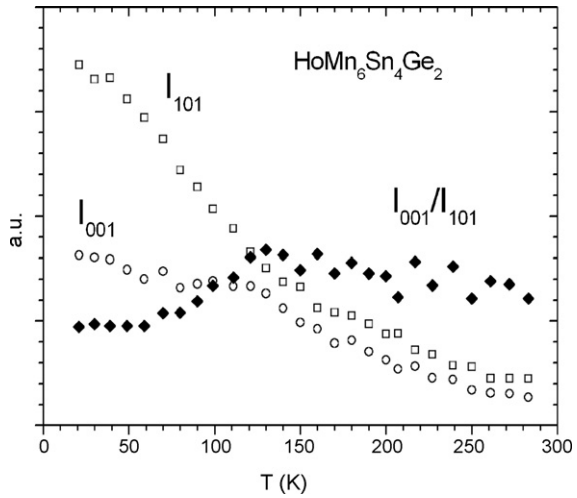

Fig. 6. Thermal variation of some characteristic lines in $HoMn_6Sn_4Ge_2$.

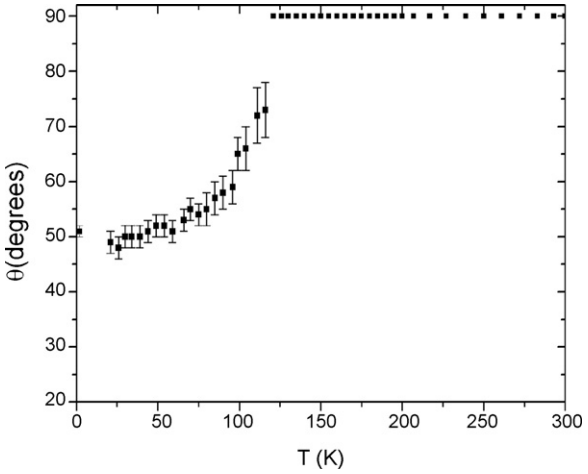

Fig. 7. Thermal variation of the angle θ between the moments and the c axis.

significantly deviates from 90° only below T_{SR} = 120 K (Fig. 7). Above this temperature, the angle is close to 75° with a large standard deviation and has been fixed to 90° without enhancing the reliability factor. The Mössbauer spectroscopy results reported in Section 3.2 confirm this behaviour. The amplitude of the Mn moment slowly decreases in the 2–300 K temperature range while the Ho moment strongly decreases (Fig. 4). The 2 K value of the holmium moment is slightly reduced with respect to the free ion value (Table 3).

3.1.4. *Magnetic structures of $LuMn_6Sn_4Ge_2$*

The pattern recorded at 2 K (Fig. 8) is characterized by additional lines which may be indexed as satellites of the nuclear ones with a propagation vector $Q = (0, 0, q_z)$ as previously observed in many other LMn_6Sn_6 and LMn_6Ge_6 compounds [4,5]. According to these preliminary remarks, the magnetic structure was initially refined assuming a helimagnetic structure consisting of an arrangement of ferromagnetic (0 0 1) planes, with the moment rotating in the successive planes along the c axis (Fig. 3). The refined parameters are the magnitude of the Mn moments, the phase angle between the moments of Mn atoms lying in $z = 1/4$ and 3/4 (defined as ϕ_{Mn} for Mn lying in $z = 1/4$ and $-\phi_{Mn}$ for Mn lying in $z = 3/4$) and the tilt angle θ_{Mn} of the normal to the helical plane with respect to the [0 0 1] direction. While this model leads to rather low residual fac-

Table 3
Structural and magnetic parameters of $HoMn_6Sn_4Ge_2$ at 300, 200 and 2 K.

	300 K	200 K	2 K
a (Å)	5.400(1)	5.387(1)	5.374(1)
c (Å)	8.705(1)	8.691(1)	8.676(1)
z_{Mn}	0.2334(7)	0.2339(8)	0.2334(9)
z_{Sn2e}	0.3337(8)	0.334(1)	0.335(1)
Occ_{Sn2d}	1	1	1
Occ_{Ge2c}	0.99(1)	0.99(1)	0.99(1)
Occ_{Sn2e}	1	1	1
μ_{Mn} (μ_B)	1.73(5)	2.07(8)	2.28(6)
μ_{Tb} (μ_B)	2.81(7)	4.86(8)	9.26(10)
θ_c (°)	90	90	51(1)
R_{Bragg}; R_f	2.55; 2.48	1.84; 0.96	2.38; 3.36
R_{magn}; χ^2	4.34; 8.2	3.36; 16.8	2.72; 15.6

Table 4
Structural and magnetic parameters of $LuMn_6Sn_4Ge_2$ at 300 and 2 K.

	300 K	2 K
a (Å)	5.384(1)	5.362(1)
c (Å)	8.676(1)	8.647(1)
z_{Mn}	0.2319(7)	0.2318(5)
z_{Sn2e}	0.3287(8)	0.3311(6)
Occ_{Sn2d}	1.00(1)	1.00
Occ_{Ge2c}	0.98(1)	0.98
Occ_{Sn2e}	1.00(1)	1.00
μ_{MnH1} (μ_B)	1.17(3)	1.97(3)
ϕ_{MnH1} (°)	28.7(9)	22.7(5)
θ_{MnH1} (°)	0	0
q_{z1}	0.382(1)	0.2778(5)
μ_{MnH2} (μ_B)	0.92(4)	1.12(5)
ϕ_{MnH2} (°)	21(1)	18(1)
θ_{MnH2} (°)	0	0
q_{z2}	0.312(3)	0.250(1)
μ_{MnAF} (μ_B)	0.26(1)	–
θ_{MnAF} (°)	90	–
μ_{Mn} (μ_B)	1.51(7)	2.27(5)
R_{Bragg}; R_f; χ^2	1.19; 1.17; 6.92	1.26; 1.28; 5.95
R_{H1}, R_{H2}, R_{AF}	21.8; 22.8; 12.8	8.04; 11.7; –

tors, it fails to account fully for the observed line-shapes. In the final refinements, a second propagation vector with a slightly reduced q_z value was introduced leading to a better calculated profile. The final parameters are gathered in Table 4 and the observed and calculated pattern is displayed in Fig. 8. Attempts to fix the helical plane perpendicular to the [0 0 1] direction ($\theta_{Mn} = 0°$) do not strongly changes the values of the residual factors: ($R_{m1} = 8.00\%$; $R_{m2} = 11.8\%$) compared with ($R_{m1} = 7.70\%$; $R_{m2} = 12.0\%$) for a free angle ($\theta_{Mn} = 19(1)°$).

The pattern recorded at 300 K is more complicated and is characterized by an enhanced splitting of the satellites (Fig. 8). In addition some weak lines are also observed between the main satellites. These lines are compatible with the antiferromagnetic structure characterized by a doubling of the c axis which is stable in $LuMn_6Sn_6$ and $TmMn_6Sn_6$ at high temperatures [4,12,13]. The observation of the (0 0 l) lines indicates that the moments are not aligned along the [0 0 l] direction. Refinements have been undertaken considering a mixing of two helimagnetic phases and one antiferromagnetic structure. The final parameters are gathered in Table 4 and the observed and calculated pattern is displayed in Fig. 8. A representation of the magnetic structures is given in Fig. 3. As for the low temperature refinements, we observed that refinement of the tilt angle does not significantly improve the reliability factors. The thermal evolution of the Mn magnetic moment and of the propagation vector components are displayed in Figs. 4 and 9. The remaining lines related to the antiferromagnetic structure which are only observed in the highest temperature patterns suggest that such an antiferromagnetic order is stable above the room temperature.

Remark: Due to the z_{Mn} position of manganese close to 1/4 in LMn_6Sn_6 and LMn_6Ge_6, compounds, the value of the phase ϕ_{Mn} is often measured with rather poor accuracy in the compounds of non magnetic L elements (L = Sc, Y, Lu). This is a crucial problem since this value is directly related to the observed arrangements of the Mn moments within the Mn–X–X–X–Mn and Mn–(X,L)–Mn slabs which, in turn, provide information on the relative strength of the Mn–Mn couplings in these two slabs. In $LuMn_6Sn_4Ge_2$, the z_{Mn} position (Table 1) is sufficiently shifted from $z = 1/4$ to allow good accuracy in the measurement of ϕ_{Mn}. An attempt to change the sign of ϕ_{Mn} and, in turn, the arrangements of the Mn moments within the Mn–Sn–Sn–Sn–Mn and Mn–(Ge,L)–Mn slabs leads to an increase of the residual magnetic factor from 12% to 49%. Therefore, in $LuMn_6Sn_4Ge_2$, we unambiguously observe that an almost ferromagnetic arrangement prevails in the Mn–Sn–Sn–Sn–Mn slab while the angle between the Mn moments belonging to the Mn–(Ge,L)–Mn slab is relatively open. The same observation applies

Table 5
Fitted values for the isomer shift IS, transferred hyperfine field, B_{hf}, quadrupole shift, ε, quadrupole splitting, Δ, and angle between V_{zz} and B_{hf}, θ at 12 K in $LMn_6Sn_4Ge_2$(L = Tb, Ho, Lu). *Note*: (–) indicates that the parameter was not used, while values in brackets "(. . .)" were either fixed or assumed in the analysis.

Compounds	Isomer shift (mm/s) IS			Hyperfine field (T) B_{hf}			Quadrupole shift (mm/s) ε			Quadrupole splitting (mm/s) Δ		θ (°)	
Site	2(c)	2(d)	2(e)	2(c)	2(d)	2(e)	2(c)	2(d)	2(e)	2(d)	2(e)	2(d)	2(e)
$TbMn_6Sn_4Ge_2$	1.8(2)	2.21(2)	2.07(2)	32.88(23)	24.95(3)	14.31(2)	–	−0.70(2)	−0.16(2)	–	–	(90)	(90)
$HoMn_6Sn_4Ge_2$	2.3(3)	2.20(2)	2.09(2)	37.85(46)	27.12(3)	14.47(4)	–	–	–	+1.55(3)	+0.37(3)	46.3(9)	52(4)
$LuMn_6Sn_4Ge_2$	1.92(7)	2.17(2)	2.10(2)	23.84(14)	25.89(3)	17.85(2)	–	−0.66(3)	(0)	–	–	(90)	(90)

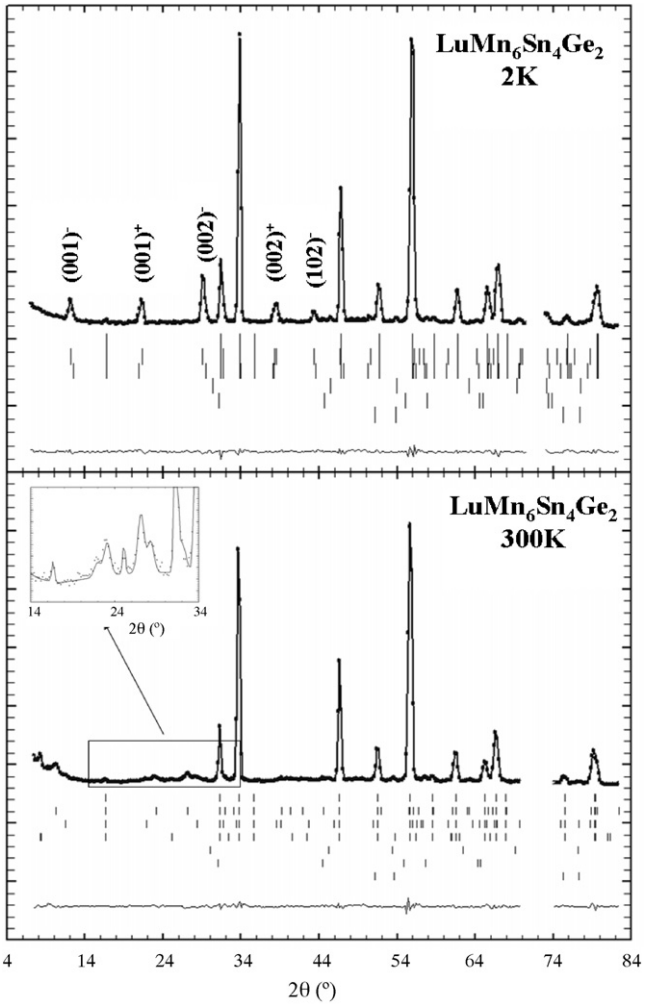

Fig. 8. Observed and calculated neutron diffraction spectra of $LuMn_6Sn_4Ge_2$ at 2 and 300 K. Insert shows the splitting of the satellites at 300 K. The three lower lines of ticks correspond to the impurities: (from bottom to top) Sn, $MnSn_2$, Mn_3Sn.

for the AF structure occurring around the room temperature: inverting the moment arrangements in the Mn–Sn–Sn–Sn–Mn and Mn–(Ge,L)–Mn slabs leads to an increase of the corresponding residual factor from 12% to 34%.

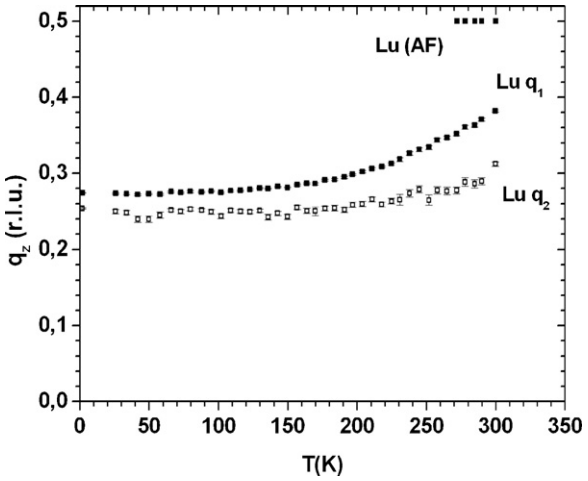

Fig. 9. Thermal variation of the q_z components of the propagating vector.

3.2. Mössbauer results

3.2.1. $TbMn_6Sn_4Ge_2$

The ^{119}Sn Mössbauer spectra of $TbMn_6Sn_4Ge_2$ (Fig. 10a) exhibit no major changes on cooling, beyond the expected monotonic increase in B_{hf} and the increasing intensity of the central component due to the metallic tin impurity phase. The fitted temperature dependences of the hyperfine fields and quadrupole shifts (ε) shown in Fig. 10b exhibit no changes that could be attributed to a change in magnetic structure, and the values of ε at each of the three sites are consistent with the easy-plane arrangement of the moments deduced from neutron scattering (REF) (Table 5).

3.2.2. $HoMn_6Sn_4Ge_2$

Visual inspection of the ^{119}Sn Mössbauer spectra of $HoMn_6Sn_4Ge_2$ presented in Fig. 11a immediately reveals a significant change in the appearance of the spectra on cooling below 150 K. As noted earlier, a slightly different approach was taken in fitting these spectra so that the angle, θ, between B_{hf} and V_{zz} (which is parallel to the crystallographic c axis) could be obtained directly from the fits. It was noted during the first-order perturbation fitting, that the quadrupole shift, ε, was essentially independent of temperature down to 150 K, and that the values observed implied an easy-plane moment arrangement. These results are fully consistent with the magnetic structure determined above by neutron scattering. In setting up the full Hamiltonian fits, we fixed θ to be 90° for the spectra 300 K > T > 150 K and determined the quadrupole interaction at the Sn(2d) and Sn(2e) sites, Δ. (Note: the intensity of the Sn(2c) component was too weak to permit this analysis for the third site as it is almost fully occupied by Ge atoms) For the spectra taken below 150 K, Δ was fixed to the average determined above 150 K and θ was allowed to vary. The results of this analysis are shown in Fig. 11b.

The most immediate observation in Fig. 11b is that θ departs from 90° for both Sn sites below 150 K. The change is initially quite rapid but tends to saturate below 50 K. The average angle at 12 K is: $\theta = 49(2)°$, which compares extremely well with the $\theta_c = 51(1)°$ deduced above from neutron diffraction data at 2 K. Additional changes are also apparent in B_{hf}. While the hyperfine field at the Sn(2d) and Sn(2c) sites increase steadily on cooling, with a possible break in slope as the moments tilt below 150 K, the drop in B_{hf} at the Sn(2e) site is extremely clear. Similar changes have been noted at this site as the magnetisation rotates from planar to axial and have been attributed to the effects of the anisotropic contribution to the transferred hyperfine field in this compound family [9,14]. The drop in field at the Sn(2e) site below 150 K provides further confirmation of changes in the spin arrangement deduced from both neutron diffraction and the electric field gradient.

3.2.3. $LuMn_6Sn_4Ge_2$

The lines in the ^{119}Sn Mössbauer spectra of $LuMn_6Sn_4Ge_2$ (Fig. 12a) were visibly broader than for the other two compounds studied here, and as a result the spectra exhibit much poorer definition. Despite this reduced resolution, it is clear from the temperature dependence of both B_{hf} and ε shown in Fig. 12b that there are no major magnetic rearrangements in the temperature range studied here (12–320 K), while the values of ε deduced from the fits suggest an easy-plane arrangement of the Mn moments [9]. These observations are fully consistent with the planar helical structure determined above by neutron scattering. A helical arrangement of magnetic moments leads to a range of magnetic environments for the three crystallographically distinct tin sites and where this range is not too broad, as is the case here, we expect to observe magnetic sextets with an increased linewidth. The axially symmetric electric field gradient that is present at each of the three Sn sites has its principal axis parallel to the crystallographic c axis, and only the angle,

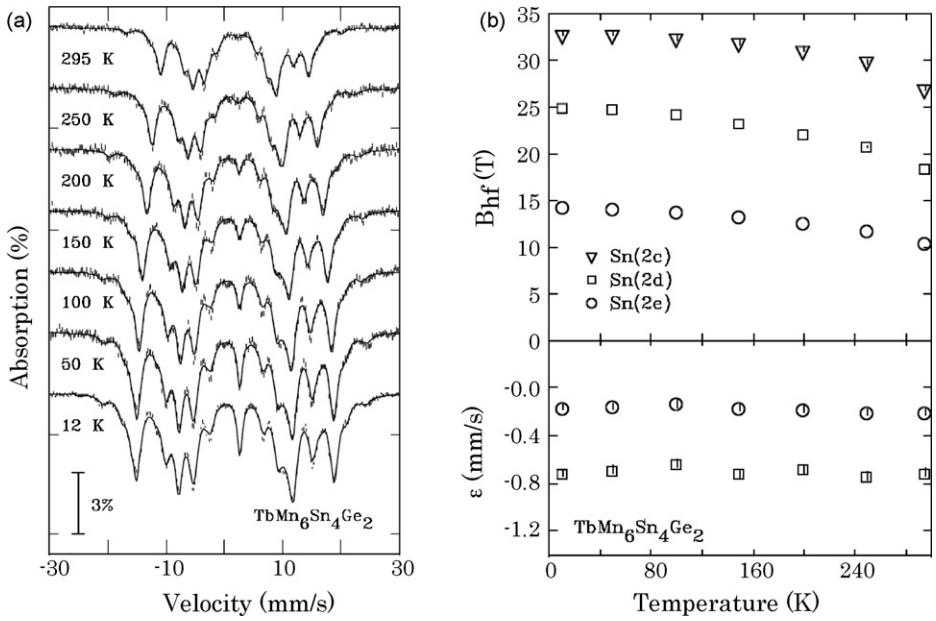

Fig. 10. ^{119}Sn spectra of $TbMn_6Sn_4Ge_2$ compounds (a) and thermal evolution of the hyperfine parameters (B_{hf} and ε) (b).

θ, with respect to this axis has any impact on the observed value of ε. As the magnetic structure deduced from neutron diffraction places all of the moments in the ab-plane, θ is 90° at all places along the spiral so easy-plane values for ε are seen in Fig. 12b. By 300 K, the magnetic splitting is greatly reduced and when combined with the broad lines that make up the observed sextets, there is insufficient resolution in this and the 320 K spectrum to permit any analysis that might detect the complex mixed helical structure that develops in the neutron diffraction data above 300 K.

4. Discussion

Our neutron diffraction and ^{119}Sn Mössbauer study of some $LMn_6Sn_4Ge_2$ compounds provides complementary information concerning the evolution of the magnetic properties with the replacement of tin by germanium.

The first remark deals with the lutetium compound. We observe that the substitution of germanium for tin does not drastically change the overall behaviour of the Mn sublattice with respect to that previously observed in the ternary $LuMn_6Sn_6$ compound [12,13]. In each case, a high temperature antiferromagnetic structure is stable and a transition from antiferromagnetism to helimagnetism takes place upon cooling. The main change concerns the transition temperature which is around 225 K for the ternary $LuMn_6Sn_6$ compound [15] and above the room temperature for the substituted $LuMn_6Sn_4Ge_2$ compound. This suggests that the relative strength of the various Mn–Mn interlayer magnetic interactions does not drastically change with the substitution. The reduction of the high temperature AF range and the smaller value of the propagation vector observed in $LuMn_6Sn_4Ge_2$ suggest a slight reduction of the AF character of this compound with respect to the parent compound $LuMn_6Sn_6$ ($q_z \approx 0.33$ at LHT) [13]. This is quite surprising

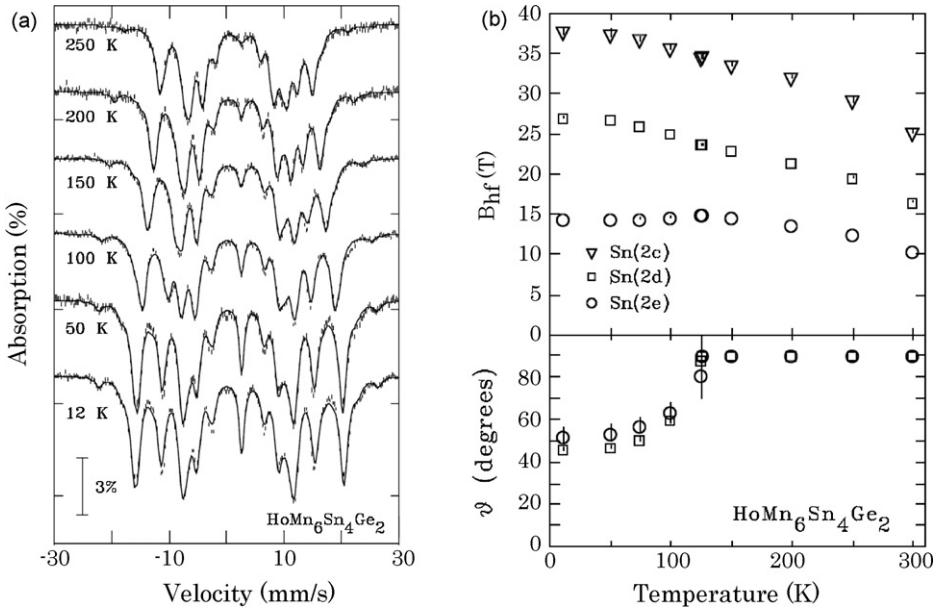

Fig. 11. ^{119}Sn spectra of $HoMn_6Sn_4Ge_2$ compounds (a) and thermal evolution of the hyperfine parameters (B_{hf} and ε) (b).

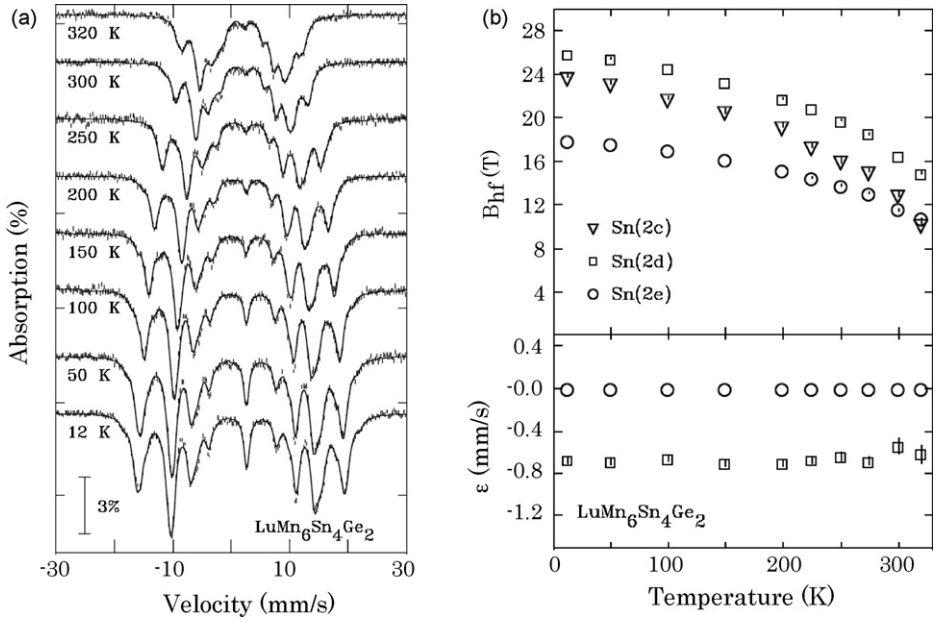

Fig. 12. ^{119}Sn spectra of $LuMn_6Sn_4Ge_2$ compounds (a) and thermal evolution of the hyperfine parameters (B_{hf} and ε) (b).

since according to previous observations, $LuMn_6Ge_6$ is characterized by a significantly stronger AF character than $LuMn_6Sn_6$. Firstly, $LuMn_6Ge_6$ remains AF in the whole ordered range [16]. Secondly, high field magnetisation measurements have shown that the critical field is smaller in $LuMn_6Sn_6$ ($B_c \approx 25$ T) than in $LuMn_6Ge_6$ ($B_c > 50$ T) [15,17]. This apparent contradiction could arise from the preferential location of the Ge atoms on the 2(c) site and may be interpreted on the basis of geometrical considerations. According to Rosenfeld et al. [18], who have developed a model based on the three main interlayer interactions in this kind of compound (Cf. Fig. 1), a helical magnetic structure is stable for $J_1 \cdot J_2 \cdot J_3 < 0$. In the case of the H_1 structure of $LuMn_6Sn_6$, the observed moment angles between the successive Mn layers are related to positive J_1 and J_2 interactions and a negative J_3 interaction and the structure is stable over a limited range of the ratio J_2/J_3. An increase in the ratio J_2/J_3 (in absolute value) leads to the stabilisation of a ferromagnetic structure while a decrease leads to the stabilisation of the antiferromagnetic AF2 structure. Since the strength of the interlayer interactions is related to the corresponding interlayer distances, and the ordering of the Ge atoms on the 2(c) site, the concomitant shift of the z_{Mn} coordinate and the change in the c/a ratio lead to different change in the two interlayer spacings (h and h' in Table 1 and Fig. 1). We may expect the $J_1:J_2:J_3$ ratios to change on replacing Ge for Sn. Going from $LuMn_6Sn_6$ to $LuMn_6Sn_4Ge_2$, we find that the spacing related to the J_2 interaction decreases much more quickly ($\Delta h'/h' = -8.1\%$) than the spacing related to the J_3 interaction ($\Delta(h+h')/(h+h') = -3.3\%$) so we expect that the ratio J_2/J_3 will increase, i.e. that the AF2 structure will be less stable.

With such an assumption, it might be suggested that the stabilisation of the low temperature ferrimagnetic structure of $TmMn_6Sn_4Ge_2$ also arises from a decreasing antiferromagnetic character of the Mn sublattice. However, since the replacement of tin by germanium does not drastically change the overall magnetic behaviour of $LuMn_6Sn_4Ge_2$ with respect to the behaviour of $LuMn_6Sn_6$, stabilisation of a ferrimagnetic structure for $TmMn_6Sn_6$ at low temperature might be also related to an increase of the Tm–Mn interactions due to a shortening of the Tm–Mn distance.

Neutron diffraction and Mössbauer spectroscopy also enabled us to check the easy magnetisation direction of terbium. Thus, Tb, with negative α_j and positive β_j Steven's coefficients displays easy-plane anisotropy whereas Tm, with positive α_j and positive β_j Steven's coefficients displays easy axis anisotropy. Both indicate that the replacement of tin by germanium yields a change of the A_2^0 crystal-field parameter, a feature which has been noted earlier in Ga substituted stannides. For the $HoMn_6Sn_4Ge_2$ compound, we observe the so-called easy cone anisotropy characterized by an intermediate direction of the magnetic moment between the [0 0 1] direction and the (0 0 1) plane. Similar behaviour has been also observed in $HoMn_6Sn_{6-x}Ga_x$ ($0.14 < x < 1.89$) crystals and discussed in terms of crystal-field theory [19]. From this analysis, it has been concluded that, for Ho (negative α_j and negative β_j), the contribution of the fourth order A_4^0 crystal-field parameter should be taken into account i.e. this fourth order parameter is not negligible with respect to the second order A_2^0 parameter.

In a previous report on the behaviour of Ga substituted stannides, it has been suggested that the change of the easy magnetisation direction with substitution was related to the outer electronic configuration of gallium atoms which are located in the equatorial plane of the hexagonal Sn_2Ga_6 dipyramid (see Fig. 1) surrounding the lanthanoid atoms [19]. However, the similar evolution of the anisotropy in Ga and Ge substituted stannides suggests that the change of the easy magnetisation direction might actually be due to distortion of the local L environment caused by the smaller atomic size of Ga or Ge with respect to Sn. According to Table 1, it is worth noting that the flattening of the hexagonal Mn_{12} prism, defined as h/D (see Fig. 1), is significantly different in $LMn_6Sn_4Ge_2$ ($h/D \approx 0.75$) and in LMn_6Sn_6 compounds ($h/D \approx 0.81$).

The Mössbauer spectroscopy study of $LuMn_6Sn_4Ge_2$ yields an interesting result. In this compound, the Sn atoms mainly occupy the 2(d) and 2(e) positions and so the ^{119}Sn Mössbauer spectrum is dominated by two sites with large hyperfine fields which are similar to those observed in ferrimagnetic $TbMn_6Sn_4Ge_2$. Therefore, we conclude that the 2(d) site is surrounded by a ferromagnetic environment of Mn atoms. In the past, there have been some discussions concerning the arrangement of the Mn moments in the helimagnetic compounds as deduced from neutron diffraction [20,21]. These problems were related to the sign of the phase angle and its consequences for the magnetic arrangement in the Mn–X–X–X–Mn or Mn–(X,R)–Mn slabs. From the Mössbauer study we can ascertain that a ferromagnetic arrangement prevails in the Mn–Sn–Sn–Sn–Mn slab and a more or less open angle in the Mn–(Ge,R)–Mn slab.

A second point dealing with the ^{119}Sn Mössbauer spectroscopy is the thermal variation of the hyperfine field observed for $HoMn_6Sn_4Ge_2$. The moment reorientation process is associated with a change in the slopes of the variation of the two hyperfine fields. Below the temperature of the reorientation, we observe a slight enhancement of the 2(d) hyperfine field and a slight decrease of the 2(e) hyperfine field. Therefore, although the moment reorientation is not complete in this compound, we observe hyperfine field variations that are similar to those previously observed in several isotypic stannides where a full spin reorientation from the (0 0 1) plane to the [0 0 1] direction occurs [9,14]. This phenomenon has been explained considering a variation of the anisotropic contribution on the ^{119}Sn nucleus caused by the moment reorientation.

Extracting additional information from the values of the hyperfine field is less easy because the field transfer is affected by many parameters such as Mn moment magnitude, interatomic Mn–Sn distances, Mn moment orientation through the variation of the anisotropic contribution, angle between the surrounding Mn moments, contribution of the L moments. However, we can try to make some comparisons between the known compounds in order to get information on these different effects.

The effect of the moment magnitude may be evaluated by comparing the hyperfine fields B_{2d} and B_{2e} measured in $LuMn_6Sn_4Ge_2$ with those in the ferromagnetic compound $YMn_6Sn_{5.42}In_{0.58}$ [9]. In both compounds, the 2(d) and 2(e) sites are characterized by the same local arrangement of the Mn moments and by similar interatomic Mn–Sn distances. In $YMn_6Sn_{5.42}In_{0.58}$, the hyperfine fields at the 2(d) site (28.98 T) and at the 2(e) site (20.54 T) are significantly higher than in $LuMn_6Sn_4Ge_2$ (+12.4% and +15.3% respectively). This enhancement should be related to the increase of the Mn moment (μ_{Mn} = 2.60 and 2.57μ_B in $YMn_6Sn_{5.63}In_{0.37}$ and $YMn_6Sn_{5.28}In_{0.72}$ respectively [22]). This moment variation (+14.5 and +13.2% respectively) fits quite well with the observed variation of the hyperfine fields.

The effect of the Mn–Sn spacings may be observed by comparing the hyperfine fields on the 2(c) site which is subjected to strong variations in the (Sn,Ge) compounds. Taking into account the only proportionality between the field and the Mn moment magnitude defined above, suggests that for the 2(c) site lying in a ferromagnetic arrangement (B_{2c} = 31.50 T in $YMn_6Sn_{5.42}In_{0.58}$) B_{hf} should be close to 29 T in a ferromagnetic $LMn_6Sn_4Ge_2$ compound. This value is significantly smaller than the values measured for the residual tin nuclei in the 2(c) site of $TbMn_6Sn_4Ge_2$ ($B_{2c} \approx 33$ T). This drastic enhancement is obviously related to the tightening of the corresponding Mn–Sn distances in this site mainly occupied by germanium atoms.

The effect of the anisotropic contribution has been already discussed above concerning the thermal variation of the hyperfine fields in $HoMn_6Sn_4Ge_2$. It can be also observed by the comparison of the field B_{2d} measured in $HoMn_6Sn_4Ge_2$ and $TbMn_6Sn_4Ge_2$. As this site is characterized by the same environment in both compounds, the larger value measured in $HoMn_6Sn_4Ge_2$ should be attributed to a larger anisotropic contribution associated to the tilting of the moment direction towards the *c* axis.

The effects of the local environment may also be seen in the values B_{2c} of the residual Sn in the 2(c) site in $LuMn_6Sn_4Ge_2$ for which a rather small hyperfine field is observed. The hyperfine field is proportional to the geometrical sum of the surrounding Mn moments which in turn is related to the value $\cos(\alpha/2)$ where α is the angle between the direction of the surrounding Mn moments. This angle is related to the refined parameters q_z and ϕ_{Mn} and takes the value $\alpha = 91.8^\circ$ for the main helimagnetic component in $LuMn_6Sn_4Ge_2$ at low temperature. For a ferro- or ferrimagnetic compound, $\alpha = 0^\circ$ and the ratio $\cos 0/\cos\alpha$ enables an estimation of the hyperfine field at the 2(c) site of a hypothetical ferromagnetic $LuMn_6Sn_4Ge_2$ compound ($B_{2c} = 23.8 \times 1.43 = 34.0$ T). This value is close to the value measured in $TbMn_6Sn_4Ge_2$ (32.88 T). Another effect of the local arrangement of the Mn moments is visible in Fig. 12. On heating the hyperfine field B_{2c} decreases more quickly than the fields B_{2d} and B_{2e}. This phenomenon is related to the thermal variation of the propagation vector component (Fig. 9): q_z increases on heating, yielding an increase of the angle α and, in turn, a decrease of the geometrical sum of the surrounding Mn moments.

The contribution of antiparallel L moments may be checked by comparing the hyperfine field at the 2(e) and 2(c) sites in $TbMn_6Sn_4Ge_2$ and $LuMn_6Sn_4Ge_2$, both compounds being characterized by the same orientation of the moments, similar moment values and similar Mn–Sn distances. For the 2(e) site, we observe a significantly smaller value in $TbMn_6Sn_4Ge_2$ ($B_{hf} \approx 14$ T compared to $B_{hf} \approx 19$ T in Lu compound). As this site is characterized by 6 ferromagnetic Mn nearest neighbours and one antiparallel Tb, it may be estimated that the Tb moment contributes −5 T at the 2(e) site. For the 2(c) site, the two compounds are not characterized by the same Mn moment arrangement, but we can use the hypothetical value estimated above for a ferromagnetic environment (B_{2c} = 34.0 T). The smaller value measured in $TbMn_6Sn_4Ge_2$ (32.88 T) suggests a negative contribution arising from the antiparallel environment of the Tb moment. There is further information provided by the comparison of the hyperfine field at the 2(e) sites in $TbMn_6Sn_4Ge_2$ and $HoMn_6Sn_4Ge_2$. Although this site is characterized by a strong anisotropic contribution to the hyperfine field [9], similar fields B_{2e} are measured in both compounds. This suggests that the negative contribution of the Tb moment is larger than the negative contribution of the Ho moment. A similar observation has been made by comparing the compounds $TbMn_6(Sn,Ga)_6$ and $ErMn_6(Sn,Ga)_6$ [8]. This indicates that the negative contribution of the L moment decreases along the magnetic lanthanoid series on going from gadolinium to thulium.

5. Conclusions

The combination of neutron diffraction and ^{119}Sn Mössbauer spectroscopy enables us to check the magnetic properties of $LMn_6Sn_4Ge_2$ compounds. Mössbauer spectroscopy always fairly well agrees with the knowledge provided by the neutron diffraction and can even provide more precise information particularly concerning the local environment of the tin atoms and the orientation of the moments. Such a combination of the two methods may be used to check the behaviour of the other members of the series. To check the contribution of the L moment (L = Gd–Tm), it would be interesting to study mixed compounds such as $Gd_{0.5}L_{0.5}Mn_6Sn_6$. In this case, the 2(e) site should experience either the negative contribution of Gd or that of L, resulting in the decoupling into two sites with different fields. However, ^{119}Sn Mössbauer spectroscopy might be also used to check the behaviour of the strongly absorbing (for neutron diffraction) compounds $GdMn_6Sn_4Ge_2$ and $SmMn_6Sn_4Ge_2$ and particularly the latter which seems to display, according to magnetisation measurements, a hard magnetic behaviour even at room temperature.

Acknowledgments

We are grateful to the Institut Laue Langevin (Grenoble) for the provision of research facilities and to Dr. Bachir Ouladdiaf for his help during the recording. DHR and LKP were supported by grants from the Natural Sciences and Engineering Research Council of Canada and Fonds Québécois de la Recherche sur la Nature et les Technologies. C.J. Voyer and E. Alonso-Ortiz (McGill) assisted with the collection of the ^{119}Sn spectra.

References

[1] G. Venturini, J. Alloys Compd. 398 (2005) 42–47.
[2] Perry S Laura K., D.H. Ryan, G. Venturini, B. Malaman, J. Alloys Compd. 469 (2009) 34–41.
[3] G. Venturini, B. Chafik El Idrissi, B. Malaman, J. Magn. Magn. Mater. 94 (1991) 35.
[4] C. Lefèvre, G. Venturini, B. Malaman, J. Alloys Compd. 346 (2002) 84–94.
[5] P. Schobinger-Papamantellos, G. André, J. Rodriguez-Carvajal, J.H.V.J. Brabers, K.H.J. Buschow, J. Alloys Compd. 226 (1995) 113.
[6] J. Rodriguez-Carvajal, Physica B192 (1993) 55.
[7] C.J. Voyer, D.H. Ryan, Hyperfine Interact. 170 (2006) 91.
[8] L.K. Perry, D.H. Ryan, G. Venturini, J. Appl. Phys. 101 (2007), 09K504_1–4.
[9] K. Laura, D.H. Perry, G. Ryan, Venturini, Phys. Rev. B75 (2007) 144417.
[10] B. Chafik El Idrissi, G. Venturini, B. Malaman, Mater. Res. Bull. 26 (1991) 431.
[11] B. Chafik El Idrissi, G. Venturini, B. Malaman, D. Fruchart, J. Less-Common Met. 175 (1991) 143.
[12] G. Venturini, R. Welter, B. Malaman, E. Ressouche, J. Alloys Compd. 200 (1993) 51.
[13] G. Venturini, D. Fruchart, B. Malaman, J. Alloys Compd. 236 (1996) 102.
[14] L.K. Perry, D.H. Ryan, G. Venturini, J.M. Cadogan, J. Appl. Phys. 99 (2006), 08J302_1–3.
[15] A. Matsuo, K. Suga, K. Kindo, L. Zhang, E. Brück, K.H.J. Buschow, F.R. de Boer, C. Lefèvre, G. Venturini, J. Alloys Compd. 408–412 (2006) 110–113.
[16] P. Schobinger-Papamantellos, G. André, J. Rodriguez-Carvajal, J.H.V.J. Brabers, K.H.J. Buschow, J. Alloys Compd. 226 (1995) 152.
[17] M. Koyama, Y. Narumi, S. Yoshii, K. Kindo, L. Zhang, E. Brück, K.H.J. Buschow, F.R. de Boer, C. Lefèvre, G. Venturini, J. Alloys Compd. 408–412 (2006) 161–163.
[18] E.V. Rosenfeld, N.V. Mushnikov, Physica B 403 (2008) 1898.
[19] C. Lefèvre, G. Venturini, J. Magn. Magn. Mater. 268 (2004) 374–379.
[20] P. Schobinger-Papamantellos, F.B. Altofer, J.H.V.J. Brabers, F.R. de Boer, K.H.J. Buschow, J. Alloys Compd. 203 (1994) 243.
[21] P. Schobinger-Papamantellos, J.H.V.J. Brabers, K.H.J. Buschow, J. Magn. Magn. Mater. 139 (1995) 119.
[22] C. Lefèvre, G. Venturini, B. Malaman, J. Alloys Compd. 361 (2003) 40–47.